Carboxylate Binding in Copper Histidine Complexes in Solution and in Zeolite Y: X- and W-band Pulsed EPR/ENDOR Combined with DFT Calculations

Debbie Baute,[†] Dafna Arieli,[†] Frank Neese,[§] Herbert Zimmermann,[‡]
Bert M. Weckhuysen,[‖] and Daniella Goldfarb*,[†]

*Contribution from the Department of Chemical Physics, The Weizmann Institute of Science,
Rehovot, Israel; Max-Planck Institute for Medical Research, Heidelberg, Germany;
Max-Planck Institute for Bioinorganic Chemistry, Mülheim an der Ruhr, Germany; and
Department of Inorganic Chemistry and Catalysis, Utrecht University, Utrecht, The Netherlands*

Received April 19, 2004; E-mail: daniella.goldfarb@weizmann.ac.il

Abstract: The complexes of copper with histidine exhibit a wide variety of coordination modes in aqueous solution. This stems from the three potential coordination sites of the histidine molecule and the existence of mono- and bis-complexes. The present work concentrates on the determination of the carboxylate binding mode, via the ^{13}C hyperfine coupling of the carboxyl, in a number of copper complexes in frozen solutions. These are then used as references for the determination of the coordination mode of two zeolite encapsulated complexes. The ^{13}C hyperfine coupling (sign and magnitude) was determined by a variety of advanced pulsed EPR and electron−nuclear double resonance (ENDOR) techniques carried out at conventional and high magnetic fields. These showed that while the carboxyl ^{13}C isotropic hyperfine coupling of an equatorially coordinated carboxylate is negative with a magnitude of 3−4 MHz, that of a free carboxylate is small (∼1 MHz) and positive. To rationalize the experimentally determined ligand hyperfine couplings (^{1}H and ^{13}C) and further understand their dependence on the coordination mode and degree of protonation, density functional theory (DFT) calculations were carried out on a number of model complexes, representing the different Cu-histidine complexes studied experimentally. The exchange-correlation functional used for the calculation of the EPR parameters was B3LYP with triple-ζ plus polarization (TZP) quality basis sets. While the polarization agreement between the magnitudes of the calculated and experimental values varied among the various nuclei, sometimes exhibiting deviations of up to 40%, an excellent agreement was found for the sign prediction. This shows the unique advantage of combining high field ENDOR, by which the sign of the hyperfine can often be determined, with DFT predictions for structure determination.

Introduction

Through the years copper−histidine complexes (CuHis) have attracted interest due to the rich coordination geometries they exhibit and the difficulties and controversies encountered in the determination of their exact structure in solution.[1] This stems from the three potential binding sites of the histidine molecule, the amino (N_a) and imidazole (N_ϵ or N_δ) nitrogen atoms and the carboxylate oxygen (O_c) (see Figure 1a), the possibility to form mono- and bis-complexes, and the dependence of the mode of coordination on the solution pH. Cu(II) binding to histidine residues is highly abundant in biological systems; histidine residues serve as ligands in most of the copper enzymes and proteins and play a role in the process of copper transport in biological systems.[2] In proteins, however, the histidine car-
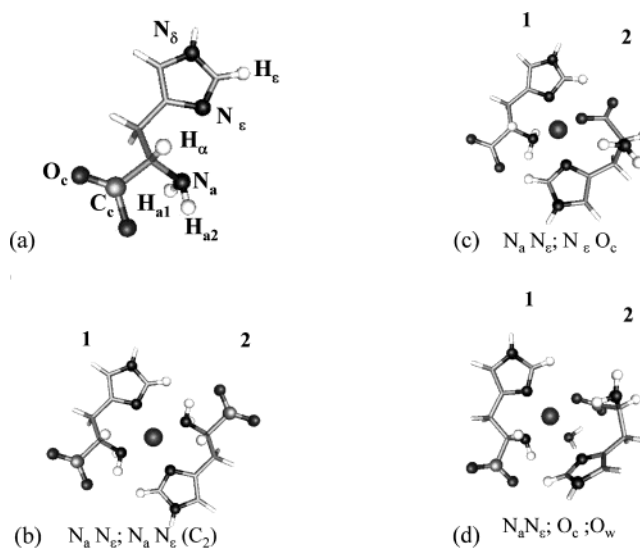
Figure 1. The Histidine molecule (a) and a few DFT optimized Cu(His)$_2$ structures with the coordination mode noted on the figure (b−d). The numbers refer to the two histidine molecules.

(1) Szabó-Plánka, T.; Rockenbauer, A.; Korecz, L.; Nagy, D. *Polyhedron* **2001**, *19*, 1123−1131 and references therein.
(2) Gray, H. B.; Solomon, E. I. In *Copper Proteins*; Spiro, T. G., Ed.; Metal Ions in Biology 3; Wiley: New York, 1981.

boxylate and amino groups are not available for coordination, although Cu(II) was found to coordinate to peptides through the backbone amide nitrogen and carbonyl group as reported for example in the prion protein.[3] In an attempt to mimic the catalytic activity of type 2 Cu(II) centers in *galactose oxidase*,[4] CuHis complexes encapsulated the pores of zeolite Y showed catalytic activity in the oxidation of alcohols and alkenes in the presence of hydrogen peroxide at ambient temperatures.[5] At least two types of CuHis complexes, each having a different coordination environment, were found, raising the question whether different coordination geometry leads to a different catalytic activity. This question can be addressed, however, only after determining the structures of the different complexes.

In earlier studies we have used a combination of ^{1}H and ^{2}H W-band (95 GHz) pulsed electron−nuclear double resonance (ENDOR) and X-band (9 GHz) electron-spin−echo envelope modulation (ESEEM) spectroscopies to determine the structure of the two different complexes in zeolite Y and of the CuHis complex in a frozen aqueous solution at neutral pH (7.3).[6,7] In the latter complex, the Cu ion is coordinated to two histidine molecules, both of which are bound through the N_a and N_ϵ nitrogen atoms (histamine-like coordination). Hence, the Cu-(II) coordination was denoted as $N_aN_\epsilon;N_aN_\epsilon$[7] (Figure 1b), where the semicolon separates coordinated atoms belonging to different histidine molecules. The same approach applied the Cu(II) complexes encapsulated in zeolite Y[6] led to the assignment of one of the complexes, termed A, to a mono-CuHis complex, having the $N_aN_\epsilon;O_w;O_z$ coordination mode, where O_w stands for a water ligand and O_z for a zeolite oxygen ligand. In this case the proximity to the zeolite framework was deduced from the observation of an intense ^{27}Al modulation in the ESEEM traces. The Cu(II) in complex B was found to be a bis-complex with the $N_aN_\epsilon;N_\epsilon O_c$ coordination mode[6] (Figure 1c), where O_c stands for the carboxylate oxygen. In these investigations, however, there was no direct evidence for carboxylate binding.

In the present work, we concentrate explicitly on the coordination of the carboxylate group in the zeolite encapsulated CuHis complexes and in frozen aqueous solutions of model complexes, using the ^{13}C hyperfine coupling of the carboxyl (C_c) as a probe. The coupling was determined by X-band two-dimensional (2D) HYSCORE (hyperfine sublevel correlation) spectroscopy and W-band pulsed ENDOR techniques and then analyzed using theoretical density functional theory (DFT) calculations. The aim of the latter was first to substantiate the coordination mode determined on the basis of the experimental ^{13}C and ^{1}H hyperfine interactions and second to design appropriate experiments that will enhance the comparison between theory and experiments. An example is the use of the absolute sign of the hyperfine splitting, which can often be determined by high field ENDOR at low temperatures.[8,9] When the anisotropic hyperfine interaction can be described by the

point-dipole approximation, the extraction of the structural parameters from the experimentally determined values is straightforward. However, when the interaction is primarily isotropic and/or when the point-dipole approximation is not valid, the extraction of the structural parameters must rely on quantum chemical computations. Recent developments in this field, particularly the formulation of DFT,[10,11] have promoted the calculations of hyperfine interactions at a relatively low computational cost with respect to traditional ab initio techniques.[12,13] This has proved particularly relevant for transition metal containing catalysts, where the complexity of the active site almost precludes the application of high-level post Hartree−Fock theories[14−16].

The calculation of EPR parameters from DFT is a relatively recent development, in particular in the case of g-tensors.[17−24] Hyperfine couplings have been more frequently considered for organic molecules where only the Fermi contact and spin-dipolar terms need to be taken into account (for reviews, see refs 25−27). The metal hyperfine coupling is considerably more difficult to calculate by DFT due to the complex nature of the Fermi contact term in this case,[12,28] the large spin−orbit coupling contribution,[29−31] and the known difficulties of DFT to describe the ionicity of the metal−ligand bonds correctly[32−34] (for recent reviews see refs 35−37). Accordingly, despite the growing interest in the field of computational chemistry, the number of transition metal containing systems to which DFT

(3) Burns, C. S.; Aronoff-Spencer, E.; Dunham, C. M.; Lario, P.; Avdievich, N. I.; Antholine, W. E.; Olmstead M. M.; Vrielink, A.; Gerfen, G. J.; Peisach, J.; Scott, W. G.; Millhauser, G. L. *Biochemistry* **2002**, *41*, 3991−4001.
(4) Lontie, R. In *Copper Proteins and Copper Enzymes*; CRC Press: Boca Raton, FL, 1984; Vol. 1−3.
(5) Weckhuysen, B. M.; Verberckmoes, A. A.; Vannijvel, I. P.; Pelgrims, J. A.; Buskens, P. L.; Jacobs, P. A.; Schoonheydt, R. A. *Angew. Chem., Int. Ed. Engl.* **1995**, *34*, 2652−2654.
(6) Grommen, R.; Manikandan, P.; Gao, Y.; Shane, T.; Shane, J. J.; Schoonheydt, R. A.; Weckhuysen, B. M.; Goldfarb, D. *J. Am. Chem. Soc.* **2000**, *122*, 11488−11496.
(7) Manikandan, P.; Epel, B.; Goldfarb, D. *Inorg. Chem.* **2001**, *40*, 781−787.
(8) Bennebroek, M. T.; Schmidt, J. *J. Magn. Reson.* **1997**, *128*, 199−206.
(9) Epel, B.; Pöppl, A.; Manikandan, P.; Vega S.; Goldfarb, D. *J. Magn. Reson.* **2001**, *148*, 388−397.
(10) Kohn, W.; Becke, A. D.; Parr, R. G. *J. Phys. Chem.* **1996**, *100*, 12974−12980.
(11) Koch, W.; Holthausen, M. C. *A Chemist's Guide to Density Functional Theory*; Wiley-VCH: Weinheim, 2000.
(12) Munzarova, M.; Kaupp, M. *J. Phys. Chem. A* **1999**, *103*, 9966−9983.
(13) Carl, P. J.; Isley, S. L.; Larsen, S. C. *J. Phys. Chem. A.* **2001**, *105*, 4563−4573.
(14) Pierloot, K.; Delabie, A.; Ribbing, C.; Verberckmoes, A. A.; Schoonheydt, R. *J. Phys. Chem. B* **1998**, *102*, 10789−10798.
(15) Pierloot, K.; Delabie, A.; Groothaert, M. H.; Schoonheydt, R. *Phys. Chem. Chem. Phys.* **2001**, *11*, 2174−2183.
(16) Cheng, H. Y.; Yang, E.; Lai, C. J.; Chao, K. J.; Wei, A. C.; Lee, J. F. *J. Phys. Chem. B* **2000**, *104*, 4195−4203.
(17) Schreckenbach, G.; Ziegler, T. *J. Phys. Chem. A.* **1997**, *101*, 3388−3399.
(18) Malkina, O. L.; Vaara, J.; Schimmelpfennig, B.; Munzarova, M.; Malkin, V.; Kaupp, M. *J. Am. Chem. Soc.* **2000**, *122*, 9206−9218.
(19) Patchkovskii, S.; Ziegler, T. *J. Phys. Chem.* **2001**, *105*, 5490−5497.
(20) Kaupp, M.; Reviakine, R.; Malkina, O. L.; Arbuznikov, A.; Schimmelpfennig, B.; Malkin, V. *J. Comput. Chem.* **2001**, *23*, 794−803.
(21) Neese F. *J. Chem. Phys.* **2001**, *115*, 11080−11096.
(22) van Lenthe, E.; Wormer, P. E. S.; van der Avoird, A. *J. Chem. Phys.* **1997**, *107*, 2488−2498.
(23) Neyman, K. M.; Ganyushin, D. I.; Matveev, A. V.; Nasluzov, V. A. *J. Phys. Chem. A.* **2002**, *106*, 5022−5030.
(24) Rinkevicius, Z.; Telyatnyk, L.; Salek, P.; Vahtras, O.; Agren, H. *J. Phys. Chem.* **2003**, *119*, 10489−10496.
(25) Engels, B.; Eriksson, L. A.; Lunell, S. *Adv. Quantum Chem.* **1996**, *27*, 297−396.
(26) Eriksson, L. A. In *Encyclopedia Quantum Chemistry;* Schleyer P. V. R., Ed.; pp 952−958.
(27) Improta, R.; Barone, V. *Chem. Rev.* **2004**, *104*, 1231−1253.
(28) Watson, R. E.; Freeman, A. *Phys. Rev.* **1961**, *123*, 521−526.
(29) van Lenthe, E.; van der Avoird, A.; Wormer, E. S. *J. Chem. Phys.* **1998**, *108*, 4783−4796.
(30) Neese, F. *J. Chem. Phys.* **2003**, *118*, 3939−3948.
(31) Arbuznikov, A. V.; Vaara, J.; Kaupp, M. *J. Chem. Phys.* **2004**, *120*, 2127−2139.
(32) Solomon E. I.; Szilagyi, R. K.; George S. D.; Basumallick, L. *Chem. Rev.* **2004**, *104*, 419−458.
(33) Szilagyi, R. K.; Metz, M.; Solomon, E. I. *J. Phys. Chem. B* **2002**, *106*, 2994−3007.
(34) Neese, F. *J. Phys. Chem. A* **2001**, *105*, 4290−4299.
(35) Neese, F. In *The Quantum Chemical Calculation of NMR and EPR Properties. Theory and Applications*; Kaupp, M., Bühl, M., Malkin, V., Eds.; Wiley-VCH: 2004; and other chapters in the same volume.
(36) Neese, F. *Curr. Opin. Chem. Biol.* **2003**, *7*, 125−135.
(37) Neese, F.; Solomon, E. I. In *Wiley series: Magnetoscience − From Molecules to Materials*; Miller, J. S., Drillon, M., Eds.; 2003; Vol. IV, pp 345−466.

methods have been applied for calculating hyperfine interactions is still limited; hence, the validity and applicability of these methods for the interpretation of experimental hyperfine couplings in terms of structure are far from being well established.[34,38]

Munzarova and Kaupp[12] found that, for the best cases, the isotropic hyperfine coupling constants could be determined to within a 10−15% margin. Significant deviations from experimental values were observed in the calculations of ligand superhyperfine interactions, and the authors attributed these large deviations to spin polarization and spin contamination effects.[39] Reasonable results for a range of Cu(II) complexes for ligand superhyperfine couplings were found, but a tendency to overestimate the dipolar and isotropic parts due to excessive spin transfer to the ligand was noted.[34] The latter deficiency of DFT has been well-known due to the work of Solomon and co-workers.[33] Nonetheless, this and other studies have shown that the error in DFT predicted values is systematic for a given set (i.e., the selected basis set and functional). Hence, DFT can be used to predict trends in the hyperfine parameters among groups of related compounds[40,41] and help in the assignment of *g*-tensors and ENDOR signals, as demonstrated by Larsen and co-workers on various VO^{2+} complexes.[13,38,42] We also note a few recent applications of DFT based EPR parameter predictions in the case of bioinorganic model chemistry which in many cases allowed for a successful interpretation of the experimental data.[43−47]

The availability of a range of experimentally determined ^{1}H and ^{13}C hyperfine tensors for a number of related CuHis complexes therefore provides a unique opportunity for further testing the validity and limitations of DFT in predicting ligand hyperfine tensors and their dependence on the specific coordination mode. This will, in turn, motivate further improvement of the calculations.

Experimental Section

Sample Preparation. A. Synthesis of ^{13}C-Histidine. Histidine(1-^{13}C) was synthesized as follows: the labeled key-intermediate ethyl-acetamidocyanoacetate-1-[13]C (I) reacted with 4-(chloromethyl)-imidazole-hydrochloride to produce *N*-acetyl-α-cyano-1-^{13}C-histidine-ethylester, which was hydrolyzed to D,L-1-^{13}C-histidine. Intermediate I was prepared by a reaction sequence starting with 1-^{13}C-acetic acid followed by 2-bromo-1-^{13}C-acetic acid, 2-cyano-1-^{13}C-acetic acid, ethylcyano-1-^{13}C-acetate, and finally ethylacetamidocyano-1-^{13}C-acetate. The experimental details for the preparation of these intermediates are described in the literature[48−50] for various isotopomers and have been

used and modified for D,L-1-^{13}C-histidine, which was obtained in approximately 20% yield from 1-^{13}C-acetic acid. The purity of the recrystallized (EtOH) D,L-1-^{13}C-histidine was tested by TLC as well as ^{1}H and ^{13}C NMR. In the following, the labeled compounds will be referred to as ^{13}C-His. We have not observed any difference in the EPR or ENDOR spectra upon using L-histidine or D,L-histidine.

B. Solutions. The copper histidine solutions were prepared by mixing aqueous solutions of $Cu(NO_3)_2 \cdot 3H_2O$ (p.a., Merck) and L-histidine (98%, Janssen Chimica) in a molar ratio of 1:3. The pH adjustments were made with NaOH (0.01N, p.a., Merck) or HCl (0.01N, p.a., Merck) to obtain complexes at pH = 7.3 and pH/pD = 3.8/3.4. The pH was adjusted by titration, followed by low temperature EPR measurements, such that the spectrum showed the presence of only one CuHis complex besides the $Cu(H_2O)_6^{2+}$ complex. The copper glycine solutions (CuGly) were prepared by mixing aqueous solutions of $Cu(NO_3)_2 \cdot 3H_2O$ and glycine (1-^{13}C) (Cambridge Isotope Laboratories, Inc.) in a molar ratio of 1:3. All solutions were prepared in deionized water or D_2O (Cambridge Isotope Laboratories, Inc.) and were mixed with equal amounts of glycerol (BDH Chemicals Ltd.) or deuterated glycerol (Cambridge Isotope Laboratories, Inc.) to produce a glass upon freezing. The final concentration of Cu(II) in the CuHis solutions was 1.5 mM for the HYSCORE measurements and 2 mM for the ENDOR measurements. The Cu(II) concentration in the CuGly solutions was 1 mM. In the following, the CuHis complexes at pH = 7.3 and 3.8 are referred to as CuHis(7.3) and CuHis(3.8), respectively. Deuterated histidine-*d₃*-α,β and glycine(1-^{13}C) were purchased from Cambridge Isotope Laboratories, Inc. and are referred to as His-*d₃* and ^{13}C-Gly.

C. Zeolite Y. A sample with a majority of complex A was prepared as follows:[5] 200 mg of zeolite Y (TSZ) with a Si/Al ratio of 2.71 were stirred in 200 mL of deionized water for 3 h at pH 7.3. The adjustments were made with HCl. A 1:3 molar ratio of a Cu(II)/histidine solution, 4 mM in Cu, was added to give a final concentration equivalent to 0.1 Cu per unit cell (UC). The pH was kept at 7.3 throughout the ion exchange and the solution was stirred for 24 h, afterwards the product was collected by suction filtration and dried at 60 °C. When necessary, remnants of complex B were removed by stirring the samples in 0.0125 N NaCl (Frutarom Laboratory Chemicals) for 10 min (the lower the loading of CuHis, the more complex A prevails[6]). The same procedure was applied for the preparation of a zeolite sample with complex B with the exception that the amount of CuHis solution was 15 times larger to obtain a loading of 1.5 Cu/UC. The preparation of samples with labeled histidine was identical to that described above.

Spectroscopic Measurements. Continuous wave (CW) X-band (9.2 GHz) EPR measurements were performed on a Varian E12 spectrometer at 150 K. The HYSCORE experiments were carried out on an X-band home-built pulse spectrometer[51,52] at 8.5 GHz and 4.5 K with the pulse sequence π/2-τ-π/2-t_1-π-t_2-π/2-τ-echo and a four step phase cycle.[53] The microwave pulse length, t_{MW}, of both the π/2 and the π pulse was 0.03 μs, the dwell time in t_1 and t_2 was 0.04 μs, and 150 × 150 points were collected (128 × 128 points for the CuGly spectrum). The treatment of the HYSCORE data was as follows: baseline correction in both t_1 and t_2 dimensions, followed by apodization with a Hamming window and zero filling to 512 points in each dimension. Then, Fourier transformation in both dimensions was carried out, and the 2D magnitude spectrum was calculated. The HYSCORE spectra are presented as contour plots with linear scaling of the contour intervals. All these manipulations were carried out with Matlab (The MathWorks, Inc.).

W-band pulsed EPR and ENDOR experiments were carried out at 94.9 GHz at ~10 K on a home-built spectrometer.[54] Some of the [13]C

(38) Larsen, S. C. *J. Phys. Chem. A* **2001**, *105*, 8333−8338.
(39) Munzarova, M.; Kubacek, P.; Kaupp, M. *J. Am. Chem. Soc.* **2000,** *122*, 11900−11913.
(40) Munzarova, M.; Kaupp, M. *J. Phys. Chem. B* **2001**, *105*, 12644−12652.
(41) Arieli, D.; Delabie, A.; Groothaert, M.; Pierloot, K.; Goldfarb, D. *J. Phys. Chem. B* **2002**, *106*, 9086−9097.
(42) Saladino, A. C.; Larsen, S. C. *J. Phys. Chem. B* **2003**, *107*, 1872−1878.
(43) Jaszewski, A. R.; Jezierska, J. *Chem. Phys. Lett.* **2001**, *343*, 571−580.
(44) Garcia Serres, R.; Grapperhaus, C. A.; Bothe, E.; Bill, E.; Weyhermüller, T.; Neese, F.; Wieghardt, K. *J. Am. Chem. Soc.* **2004**.
(45) Sinnecker, S.; Noodleman, L.; Neese, F.; Lubitz, W. *J. Am. Chem. Soc.* **2004**, *126*, 2613−2622.
(46) Sinnecker, S.; Neese, F.; Lubitz, W. *J. Am. Chem. Soc.* **2004**, *126*, 3280−3290.
(47) Van Gastel, M.; Lassman, G.; Lubitz, W.; Neese, F. *J. Am. Chem. Soc.* **2004**, *126*, 2237−2246.
(48) SooHoo, C.; Lawson, J. A.; DeGraw. J. I. *J. Labeled Compds.* **1977**, *13*, 97−102.
(49) Ott, D. G. *Synthesis with stable isotopes.* Wiley-Interscience & Sons: New York, 1981; pp 33, 35, 161.
(50) Murray, A.; Williams, D. L. *Organic synthesis with Isotopes.* Interscience: New York, 1958; pp 294−296, 442−443.
(51) Goldfarb, D.; Fauth, J. M.; Tor, Y.; Shanzer, A. *J. Am. Chem. Soc.* **1991**, *113*, 1941−1948.
(52) Shane, J. J.; Gromov I.; Vega, S.; Goldfarb, D. *Rev. Sci. Instrum.* **1998**, *69*, 3357−3364.
(53) Fauth, J. M.; Schweiger, A.; Braunschweiler, L.; Forrer J.; Ernst, R. R. *J. Magn. Reson.* **1986**, *66*, 74−85.
(54) Gromov, I.; Krymov, V.; Manikandan, P.; Arieli, D.; Goldfarb, D. *J. Magn. Reson.* **1999,** *139*, 8−17.

and all ^2H ENDOR spectra were recorded using the Mims ENDOR[55] pulse sequence ($\pi/2$-τ-$\pi/2$-T-$\pi/2$-echo where a RF pulse is applied during time T). For Mims ENDOR, a t_{MW} of 0.1 μs was used and the RF pulse length, t_{RF}, was 32 μs for ^{13}C and 35 μs for ^2H. The intensity scale of the Mims spectra and the frequency scale of the ^2H spectra were multiplied by -1 and $\gamma_H/\gamma_D = 6.5144$, respectively, to allow comparison with the ^1H ENDOR spectra. The ^1H Davies ENDOR[56] spectra (π-T-$\pi/2$-τ-π-τ-echo with a RF pulse during time T) were acquired with $t_{RF} = 15$ μs and $\tau = 0.5$ μs. The ^{13}C Davies ENDOR spectra were recorded with $t_{RF} = 35$ μs, and all ^{13}C spectra were recorded using random acquisition.[57] The sign of the hyperfine coupling was determined using the variable mixing time (VMT) ENDOR experiment, where an additional time interval, t_{mix}, is introduced after the RF pulse.[8,9] The orientation selective ^{13}C Davies ENDOR spectra were recorded with the Special TRIPLE sequence.[57,58] This experiment is similar to the Davies sequence, but instead of one RF π pulse, two RF π pulses are applied and their frequencies are scanned symmetrically with respect to the nuclear Larmor frequency, ν_I, such that the ENDOR transitions of the two $M_S = \pm^1/_2$ manifolds are on resonance. This experiment gives an enhancement of a factor of 2 in the ENDOR effect. This set of spectra was acquired with $t_{RF} = 32$ μs and $\tau = 0.40$ μs. In all Davies VMT ENDOR and Special TRIPLE experiments, t_{MW} of 0.2 and 0.1 μs were used for the π and $\pi/2$ pulses, respectively.

Simulations. Spectral simulations were carried out with a program developed in house using Matlab. The ENDOR frequencies of the simple case of an electron spin, $S = ^1/_2$, coupled to an $I = ^1/_2$ nuclear spin are determined from the following Hamiltonian:

$$\hat{H} = \frac{\beta}{h}\vec{B}\cdot\mathbf{g}\cdot\hat{S} - \frac{g_n\beta_n}{h}\vec{B}_0\cdot\hat{I} + \hat{S}\cdot\mathbf{A}\cdot\hat{I} \qquad (1)$$

where the first and second terms describe the electron spin and nuclear spin Zeeman interactions, respectively, and the third term represents the hyperfine interaction. It is convenient to express $\vec{B}$ and $\mathbf{A}$ in the principal axis system of the g-tensor (X,Y,Z). Accordingly, $\mathbf{A}$ is characterized by its principal components, A_{xx}, A_{yy}, A_{zz} (or $A_{\parallel}$ and $A_{\perp}$ for an axially symmetric tensor), and the Euler angles α, β, and γ, which relate the $\mathbf{A}$ principal axes system (x,y,z) to that of the $\mathbf{g}$ principal axes system. When $\mathbf{g}$ is axially symmetric, α can be set to zero. The anisotropic part of $\mathbf{A}$ is represented by $\mathbf{T}$, and the isotropic part, by a_{iso}. The first-order expressions for the ENDOR frequencies for a weak coupling case, which usually holds for protons at high fields, are

$$\nu_{\alpha,\beta} = \nu_I \mp 0.5A \qquad (2)$$

where $\nu_I = g_n\beta_n/h\ B_0$ is the nuclear Larmor frequency and A is the hyperfine coupling. The latter is a function of β, γ, and the orientation of $\vec{B}$ with respect to (X,Y,Z) is given by θ_0 and ϕ_0.[59]

For electron–nuclear distances, r, greater than 2.5 Å, and when the spin delocalization over the ligand is negligible, $T_\perp = -0.5T_{zz} = T_{xx} = T_{yy}$ and it can be described by the point-dipole approximation:

$$T_\perp = \frac{\mu_0\rho^{\alpha-\beta}}{4\pi}\frac{g_e\beta_eg_n\beta_n}{r^3} \qquad (3)$$

where $\rho^{\alpha-\beta}$ is the spin density. When pulsed EPR experiments are carried out on a sample exhibiting a powder pattern, as in the case of g-anisotropy, only a selected range of θ_0 and ϕ_0 orientations, determined by the field position within the spectrum, contribute to the spectrum. These selected orientations can be obtained from simulations of the

field sweep echo detected EPR spectrum, taking into account the line width and the MW pulse bandwidth.[51,60,61]

Computational Methods. A. Geometries and Relative Stabilities. Gas-phase full geometry optimizations were carried out with DFT,[10] using the Turbomole code version 5.3.[62] The three parameter Becke exchange functional[63] and the Lee–Yang–Parr[64] correlation functional, i.e., the combination commonly denoted as B3LYP, were employed in all cases. Basis sets from Schäfer et al.[65] were employed: For Cu, a double-ζ basis set was chosen and enhanced with p, d, and f functions (with exponents 0.174, 0.132, and 0.390, respectively, according to Pierloot et al.[15]). The coordinating nitrogen/oxygen atoms were described by a double-ζ basis set which was enhanced by one polarization function (DZP), while for all other atoms double-ζ basis sets (DZ) were selected. The convergence criteria used were 10^{-6} Hartree for the energy change and 10^{-3} Hartree/Bohr for the gradients. Starting geometries for the bis-complexes (no water included) were generated by Cerius (using the D-histidine configuration). All other starting geometries were manually adjusted from the latter according to the relevant coordination mode. In cases of complexes differing only by the degree of protonation, the optimization was usually carried out in steps, in which the nonprotonated complex was optimized first and then modified to generate the starting model of the protonated structure.

All gas-phase optimizations were done under no symmetry constraints, except for the following: the $N_aN_\epsilon;N_aN_\epsilon$ type was optimized both in its trans (C_2 and C_i) and cis (C_s) configurations, the four coordinated $[N_aN_\epsilon;N_aN_\epsilon]^{++}$ and six-coordinated $N_aN_\epsilon;O_w;N_aN_\epsilon;O_w$ complexes were optimized under C_2 symmetry, and the six-coordinated $N_aN_\epsilon O_c;N_aN_\epsilon O_c$ complex was optimized under C_i symmetry. Optimization of the trans $N_aN_\epsilon;N_aN_\epsilon$ complex in solution and all single-point calculations of the energy in solution were done with no symmetry constraints using the conductor-like screening solvation model, COSMO,[66,67] as implemented in the Turbomole code, with a dielectric constant, $\epsilon = 80$.

The stability of the hydrated complexes was calculated using the following scheme:

$$Cu(His)_2 + xH_2O \rightarrow Cu(His)_2 \cdot xH_2O \qquad (4)$$
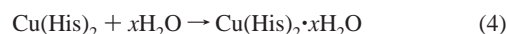
where $x = 1$ or 2. All components in eq 4 were optimized, and the relative stability of the product was calculated by subtracting the energies of the reactants. As explained above, these calculations were done both for the gas-phase energies as well as for the COSMO energies, obtained in aqueous solution.

B. Hyperfine Coupling Constants and Spin Densities. All-electron DFT calculations of hyperfine coupling and g-tensors were done using the recently developed methodologies that are implemented in the ORCA code version 2.2.[68] The calculations for the $N_aN_\epsilon;N_aN_\epsilon$ (C_2) complex were done at several theory levels to test the effect of increasing the size of the basis set and changing the type of the functional (see Supporting Information). Based on this test, the functional B3LYP and the basis set, referred to as TZP, which includes the CP(PPP) basis[69] for the copper and triple-ζ enhanced with one polarization function for all other atoms were chosen. The criterion was the agreement with the experimental hyperfine couplings available

(55) Mims, W. B. *Proc. R. Soc. London* **1965**, *283*, 452–457.
(56) Davies, E. R. *Phys. Lett. A* **1974**, *47*, 1–2.
(57) Epel, B.; Arieli, D.; Baute, D.; Goldfarb, D. *J. Magn. Reson.* **2003**, *164*, 78–83.
(58) Kurreck, H.; Kirste, B.; Lubitz, W. *Electron Nuclear Double Resonance Spectroscopy of Radicals in Solution*; VCH Publishers: New York, 1988; Chapter 3.
(59) Jeschke, G.; Spiess, H. W. *Chem. Phys. Lett.* **1998**, *293*, 9–19.

(60) Rist, G. H.; Hyde, J. S. *J. Chem. Phys.* **1970**, *52*, 4633–4643.
(61) Hurst, G. C.; Henderson, T. A.; Kreilick, R. W. *J. Am. Chem. Soc.* **1985**, *107*, 7299–7303.
(62) Ahlrichs, R.; Bär, M.; Häsner, M.; Horn , H.; Kölmel, C. *Chem. Phys. Lett.* **1989**, *162*, 165–169.
(63) Becke, A. D. *J. Chem. Phys.* **1993**, *98*, 5648–5652.
(64) Lee, C. T.; Yang, W. T.; Parr, R. G. *Phys. Rev. B* **1988**, *37*, 785–789.
(65) Schäfer, A.; Horn, H.; Ahlrichs, R. *J. Chem. Phys.* **1992**, *97*, 2571–2577.
(66) Klamt, A.; Schürmann, G. J. *J. Chem. Soc., Perkin Trans.* **1993**, *2*, 799–805.
(67) Barone, V.; Cossi, M. *J. Phys. Chem. A* **1998**, *102*, 1995–2001.
(68) Neese, F. *ORCA- an ab initio, DFT and semiempirical porogram package*, version 2.2-74; Max Planck Institute for Bioinorganic Chemistry: Mülheim an der Ruhr, Germany, unpublished.
(69) Neese, F. *Inorg. Chim. Acta* **2002**, *337C*, 181–192.

Table 1. Summary of the *g*-Values and *A*(Cu) Values of the Species Investigated

species	$g_\parallel$	$g_\perp$	$A_\parallel$ (MHz)
$Cu(H_2O)_6^{2+}$	2.40	2.06	402
CuHis (3.8)	2.31	2.06	507
CuHis(7.3)	2.23	2.06	555
CuGly	2.31	2.07	484
CuHis A−Y[a]	2.31	2.05	510
CuHis B−Y[a,b]	2.25	2.07	576

[a] Values taken from Grommen et al..[6]　[b] Sample contains about 30% complex A.

for this complex (CuHis(7.3)) as well as computational convergence with respect to basis set size. The calculations were carried out on structures optimized in the gas phase because the solvent effects were found to be insignificant for the purpose of our study (see Supporting Information). Spin density surface plots were calculated at a $75 \times 75 \times 75$ resolution and generated using the gOpenMol program.[70] The expressions used to calculate the hyperfine and *g*-tensors are summarized in the Supporting Information.

Results and Discussion

Model Complexes in Solution. Since one of the major goals of this work was to establish the carboxylate coordination in CuHis complexes, models for equatorial and axial coordination and free COO^- were required. As a model for equatorial coordination, we used a solution of the $^{13}C-CuGly$ complex, at neutral pH, which has the $N_aO_c;N_aO_c \cdot 2H_2O$ coordination mode.[71] The second model compound was the $N_aN_\epsilon;N_aN_\epsilon$ $^{13}C-$ CuHis(7.3) complex in a frozen solution.[7] The third model was the complex which prevails, together with the aqua-complex, $Cu(H_2O)_6^{2+}$, in solutions of $^{13}C-CuHis(3.8)$, and the EPR parameters of this complex are the same as those of the encapsulated zeolite complex A. At higher pH values, other CuHis species appear. Table 1 summarizes the EPR parameters of all samples studied in this work as determined from the X- and W-band low-temperature EPR spectra.

A. HYSCORE Measurements. The HYSCORE experiment generates 2D spectra with cross-peaks that represent correlations between the ENDOR frequencies of one electron spin manifold with those of the other electron spin manifold.[72] For example, for $S = {}^1/_2$, $I = {}^1/_2$, the cross-peaks appear at (ν_α,ν_β) and (ν_β,ν_α) (see eq 2). The HYSCORE spectrum of $^{13}C-CuGly$, depicted in Figure 2a, shows a clear set of cross-peaks centered at the ^{13}C Larmor frequency, ν_C, with a width of $\sim$2.3 MHz and a splitting of 3.6 MHz (the peaks on the diagonal of the $(-,+)$ quadrant are noise). Spectra measured at 0.28 T, in the $g_\parallel$ region, showed a pair of cross-peaks with a splitting of 3.7 MHz and a width of 1.3 MHz. From the width and position of the cross-peaks in the two spectra and the low orientation selectivity at $g_\perp$, $a_{iso} \approx 3$ MHz and $T_{zz} \approx 2-3$ MHz were estimated (exact values were later obtained from the simulations of the ENDOR spectra given below). The HYSCORE spectrum of $^{13}C-CuHis-$ (3.8), recorded at $g_\perp$ and shown in Figure 2b, exhibits in addition to the typical ^{14}N cross-peaks of the imidazole remote nitrogen (N_δ) at (0.7;4.0) and (1.4;4.0) MHz,[6] ^{13}C cross-peaks at (1.4;5.2) and (5.2;1.4) MHz. From the position of these peaks, $a_{iso} \approx$

(70) Relevant documentation can be downloaded from http://laaksonen.csc.fi/gopenmol.

(71) de Bruin, T. J. M.; Marcelis, A. N. T.; Zuilhof, H.; Sudholter, E. J. R. *Phys. Chem. Chem. Phys.* **1999**, *1*, 4157−4163.

(72) Höfer, P.; Grupp, A.; Nebenführ, H.; Mehring, M. *Chem. Phys. Lett.* **1986**, *132*, 279−282.
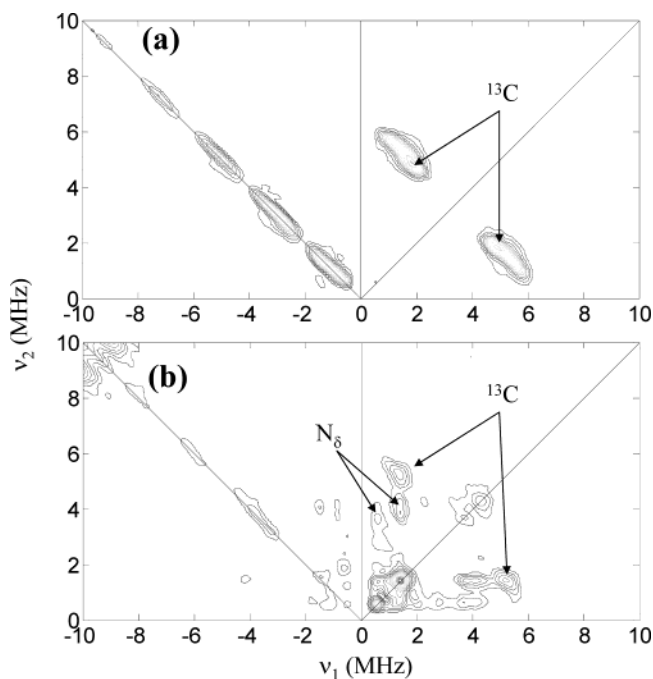
Figure 2. HYSCORE spectra of (a) $^{13}C-CuGly$ at 0.3037 T ($g_\perp$) and $\tau = 0.21$ μs, and (b) $^{13}C-CuHis(3.8)$ at 0.2960 T ($g_\perp$), $\tau = 0.19$ μs.

3.8 MHz is estimated, which is somewhat larger than that of $^{13}C-CuGly$. The similar ^{13}C coupling and the appearance of the N_δ peaks provide evidence for an equatorial coordination of both O_c and N_ϵ in the CuHis(3.8) complex. It was impossible to obtain X-band HYSCORE spectra of the second model, $^{13}C-$ CuHis(7.3), because echoes could not be observed, most likely due to deep nuclear modulations, which cause a complete echo suppression, even for short τ values. We therefore turned to pulse ENDOR measurements at W-band, where the nuclear modulation effect is usually eliminated.

B. ^{13}C W-Band ENDOR Measurements. Orientation selective Mims ENDOR spectra of the $^{13}C-CuHis(7.3)$, recorded at various fields within the EPR powder pattern, show a doublet with a splitting of 1 MHz centered at $\nu_C = 35.2$ MHz (Figure 3a). Measurements carried out at different τ values did not show any significant changes. The spectra exhibit a rather weak orientation dependence, and best fit simulations yield the ^{13}C hyperfine parameters listed in Table 2. The blind spots[73] were taken into account in the simulations by multiplying the calculated ENDOR spectrum by $\sin^2(A\tau/2)$, where A is the hyperfine coupling, as shown in Figure 3a. Motivated by the DFT calculations (see next section), we have also determined the sign of the hyperfine coupling of CuHis(7.3) by the VMT Mims ENDOR experiment,[9] as shown in Figure 4a. The reduction in the intensity of the low-frequency line with increasing t_{mix} assigns it to the α manifold. Then, using eq 2, a positive A value is obtained. This further leads to $a_{iso} > 0$, because a_{iso} is the predominant contribution to the hyperfine interaction. Here Mims VMT ENDOR was employed because it is more appropriate for small couplings than the Davies VMT ENDOR.
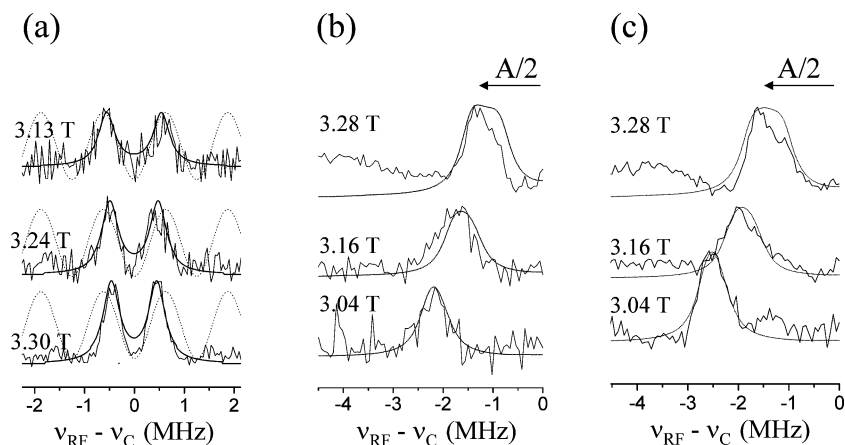
For comparison, the top trace of Figure 4a shows the ^{13}C Mims ENDOR spectrum of $^{13}C-CuHis(3.8)$ recorded at $g_\perp$, along with the pattern of the blind spots. Two doublets are

(73) Schweiger, A.; Jeschke, G. *Principles of Pulse Electron Paramagnetic Resonance*; Oxford University Press: Oxford, 2001.

Figure 3. (a) Orientation selective Mims ENDOR spectra of CuHis(7.3) recorded at $\tau = 0.40$ μs. The observer fields are noted on the figure. Simulated traces obtained with the parameters listed in Table 2 are shown as solid lines, and the function $\sin^2(A\tau/2)$ is shown as dotted lines (see text). The selected θ_0 ranges used in the simulations are (top to bottom) 75−90°, 56−69°, and 30−43°. (b) W-band Special TRIPLE spectra of a solution of ^{13}C−CuGly at three different magnetic fields, $\tau = 0.4$ μs. The solid line represents simulations (parameters are given in Table 2), and the selected ranges of θ_0 from top to bottom are 75−82°, 50−58°, and 20−38°. (c) Same conditions as those for part b except for ^{13}C−CuHis(3.8).

Table 2. Summary of All the Experimental Hyperfine Couplings [MHz] of the CuHis(Gly) Complexes

| | | | hyperfine, MHz (degrees) | |
nuclei	sample	coordination	a_{iso}, T_{xx}, T_{yy}, T_{zz}, (α, β, γ)	ref
H_{a1}	CuHis(7.3)	$N_aN_\epsilon;N_aN_\epsilon$	−9, 3, 2, −5 (0,20,90)[a]	7
H_{a2}	CuHis(7.3)	$N_aN_\epsilon;N_aN_\epsilon$	−10, 4, 0, −4 (0,84,90)[a]	7
H_α	CuHis(7.3)	$N_aN_\epsilon;N_aN_\epsilon$	10.9, −1.3, −1.3, 2.6 (0,60,0)[a]	7
H_α	CuHis B−Y	$N_aN_\epsilon;N_\epsilon O_c$	same as above	6
H_ϵ	CuHis(7.3)	$N_aN_\epsilon;N_aN_\epsilon$	0.67, −1.5, −3.1, 4.7 (0,70,0)[a]	7
C_c	CuHis(7.3)	$N_aN_\epsilon;N_aN_\epsilon$	1.0, −0.1, −0.1, 0.2 (0,0,0)	this work
C_c	CuHis(3.8)	$N_aN_\epsilon;O_c;O_w$	−3.7, −2.0, 0.2, 1.8 (0,90,50)	this work
C_c	CuHis B−Y	$N_aN_\epsilon;N_\epsilon O_c$	same as above	this work
C_c	CuGly	$N_aO_c;N_aO_c$	−3.1, −1,9, 0.2, 1.7 (0,90, 70)	this work

[a] The signs were determined according to ref 9 from the spectra and simulations appearing in the noted reference.

observed with splittings of 1.3 and 3.3 MHz, yet comparison with the Special TRIPLE spectra (Figure 3c) and the pattern of the blind spots show that the two doublet appearance is a consequence of a blind spot in the center of a single doublet. This comparison also shows that the Davies ENDOR spectra may lack some intensity in the center, due to the insensitivity of the Davies ENDOR sequence to very small couplings. This suggests the presence of an additional weakly coupled ^{13}C in CuHis(3.8).

Orientation selective W-band ENDOR measurements were carried out on both ^{13}C−CuHis(3.8) and ^{13}C−CuGly to determine more accurately the isotropic and anisotropic components of the ^{13}C hyperfine couplings. Here, the Special TRIPLE sequence was used to improve the S/N.[57] The spectra are shown in Figure 3b,c (examples of a regular Davies ENDOR of ^{13}C−CuGly can be seen in Figure 4b for comparison). The spectra of ^{13}C−CuHis(3.8) show a single ^{13}C line, the position of which shows a hyperfine splitting that increases from 3 to 5 MHz as the field changes from $g_\perp$ toward $g_{||}$, whereas for ^{13}C−CuGly it varies from 2.4 to 4.4 MHz (consistent with the HYSCORE results). DFT calculations (see next section) predicted a negative sign for the $a_{iso}(C_c)$ of an equatorially bound carboxylate as opposed to a positive one for a free carboxylate. VMT Davies ENDOR spectra of ^{13}C−CuGly recorded at $g_\perp$ are shown in Figure 4b. The top spectrum shows an asymmetric doublet, of which the line at −1.3 MHz is weaker. As t_{mix} increases, the relative intensity of this line increases, while that of the high-frequency component decreases, thus yielding a negative

coupling.[9] The asymmetry at the short t_{mix} value is a consequence of partial saturation of the NMR transitions, and the low intensity line corresponds to the β manifold,[9] consistent with the negative sign. The same behavior was observed for the ^{13}C−CuHis(3.8) solution (not shown). Using a negative hyperfine coupling, the orientation selective spectra of ^{13}C−CuGly and ^{13}C−CuHis(3.8) (Figure 3b,c) were simulated with the best fit parameters listed in Table 2, and the simulated spectra are depicted as dotted traces in Figure 3b,c.

From the ^{13}C HYSCORE and ENDOR measurements, we conclude that for an equatorial carboxylate coordination the a_{iso}-(C_c) is relatively large and negative, whereas for an axially coordinated or free carboxylate it is small and positive.

C. ^{1}H, ^{2}H W-Band ENDOR Measurements. ^{1}H and ^{2}H W-band ENDOR measurements were carried out in order to complete the determination of the coordination mode of CuHis-(3.8), specifically searching for evidence for the N_a binding to Cu(II). The spectra of natural abundance CuHis(3.8) and CuHis-d_3(3.8) in H_2O and D_2O are depicted in Figure 5. The bottom spectrum is the ^{1}H spectrum of CuHis-d_3(3.8) in H_2O, and it clearly shows the signals of H_a and H_ϵ, which are similar to those of CuHis(7.3) with the $N_aN_\epsilon;N_aN_\epsilon$ coordination mode.[7] The corresponding ^{2}H spectrum shows a clear doublet with a splitting of 10.5 MHz (in the ^{1}H frequency scale) assigned to H_α.[7,74] The ^{1}H spectrum of CuHis(3.8) in D_2O again reveals the signals of H_α and H_β, the large intensity at ν_H is absent and new features at ±1.6 MHz, not observed in CuHis(3.8),[7] become evident. The ^{2}H spectrum of this sample shows a broad powder pattern, which covers the range of both the exchangeable H_a and water ligands, as deduced from the comparison with the ^{1}H spectrum of $Cu(H_2O)_6^{2+}$ (not shown). The appearance of a water signal is expected from the contribution of the aqua-complex, which is present in the solution as well.

D. Coordination Mode of CuHis(3.8). The HYSCORE and the W-band ENDOR spectra of CuHis(3.8) identified unambiguously equatorial N_a, N_ϵ, and O_c ligands, thus concluding that this complex is a bis-complex. In this case, the H_α protons

---

(74) The similar line shape of the H_α signal in the ^{2}H and ^{1}H spectra (in the frequency scale of the latter) shows that the quadrupolar splittings are not resolved. This indicates that the inhomogeneous line width is larger than the maximum ^{2}H quadrupole splitting, which is around 0.3 MHz.
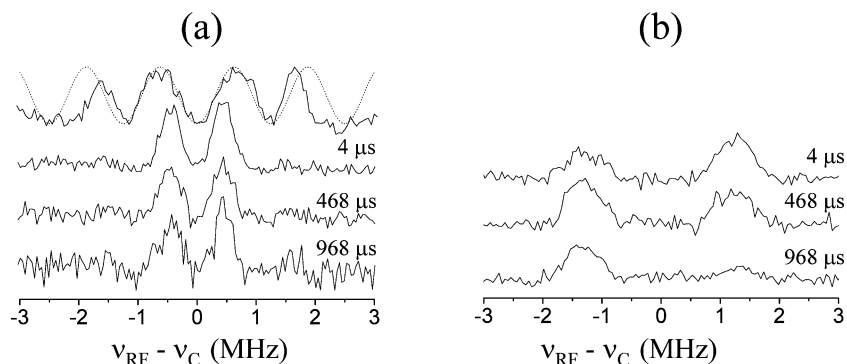
Figure 4. (a) (Bottom three traces) VMT Mims ENDOR spectra of CuHis(7.3) and Mims ENDOR (top) of ^{13}C−CuHis(3.8) superimposed on the function $\sin^2(A\tau/2)$, $\tau = 0.3$ μs. (b) VMT Davies ENDOR spectra of ^{13}C−CuGly. All spectra were recorded at $g_\perp$. The t_{mix} values are marked on each trace.
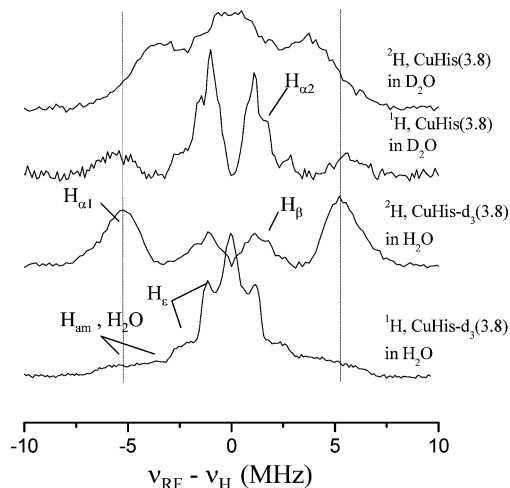
Figure 5. W-band ^{1}H (Davies) and ^{2}H (Mims) ENDOR spectra of CuHis-(3.8) recorded at the $g_\perp$ field position. The lines mark the positions of the H_α doublet. The frequency scale of the ^{2}H spectra was multiplied by γ_H/γ_D.

of the two histidine molecules should have different couplings, and consequently, we assign the doublet at ±1.6 MHz to a second H_α proton. The question that remains is which ligand atoms originate from the same molecule. We exclude the possibility of any $NNNO_c$ configuration on the basis of the A and g-values according to the Peisach−Blumbergen correlations.[75] A large a_{iso} value of H_α (∼10 MHz) was suggested earlier to be a signature for a histamine N_aN_ϵ binding mode,[7] which was supported by comparative measurements carried out on a Cu(II) 1-*methyl*-histidine complex.[7] There, the N_ϵ cannot coordinate to the Cu(II), and the coupling of H_α was found to be significantly smaller. Additional support is obtained from the smaller coupling of the H_α in CuGly.[76] Therefore, the preferred coordination mode is $N_aN_\epsilon;O_c;O_w$ (see Figure 1d). In this case, each of the histidine ligands should give rise to a different ^{13}C coupling. The presence of a ^{13}C with a small hyperfine coupling, arising from the free carboxylate, was observed in the Mims ENDOR spectrum as shown in Figure 4a (top trace). The dependence of the ^{13}C$_c$ and H_α hyperfine coupling on the chelating mode was explored in detail through DFT calculations described below.

Zeolite Complexes. The HYSCORE spectrum of the ^{13}C−CuHis zeolite complex A, shown in Figure 6a, is similar to that of the ^{13}C−CuHis(3.8) (see Figure 2), except for the appearance

(75) Peisach, J.; Blumbergen, W. E. *Arch. Biochem. Biophys.* **1974**, *165*, 691−708.
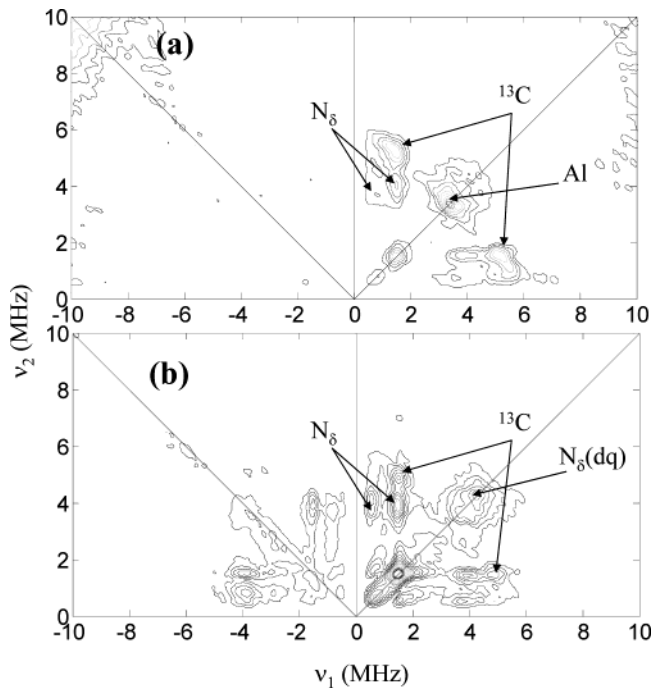
Figure 6. HYSCORE spectra of the zeolite Y ^{13}C−CuHis complexes A (a) and B (b) at the $g_\perp$ field position (0.3007 T for complex A, 0.2900 T for complex B), $\tau = 0.19$ μs. The assignments of the peaks are noted on the figure.

of an additional strong peak on the diagonal at (3.4;3.4) MHz, corresponding to the ^{27}Al Larmor frequency. This is consistent with the proximity of complex A to the zeolite framework.[6] The cross-peaks at (1.6;5.2) and (5.2;1.6) MHz are attributed to ^{13}C and, as expected, they were absent in the HYSCORE spectrum of the corresponding sample prepared with natural abundance histidine (not shown). Other cross-peaks are due to the remote N_δ. The HYSCORE spectrum of ^{13}C−CuHis zeolite complex B (see Figure 6b) is similar to that of complex A with the exception that the ^{14}N peaks are relatively stronger and the ^{27}Al peak is hardly detected. The diagonal peak at 4.0 MHz is due to double quantum frequencies of N_δ[6] resulting from incomplete inversion induced by the MW π pulse. Again, the ^{13}C cross-peaks were absent in the natural abundance sample. The HYSCORE spectra of the two complexes and the ^{13}C coupling similarity to ^{13}C−CuHis(3.8) provide direct evidence that in both complexes an equatorial O_c ligand is present.[77] The ^{1}H and ^{2}H W-band ENDOR spectra of the two complexes were

(76) Baute, D.; Goldfarb, D. Unpublished results.

Table 3. Calculated Principal Components of the Copper Hyperfine and g-Tensors for Different Complexes[a]

complex	model for	Cu hyperfine, MHz A_{xx}, A_{yy}, A_{zz}	g-tensor g_{xx}, g_{yy}, g_{zz}
$N_aN_\epsilon;N_aN_\epsilon$ (C_2)[#]	CuHis (7.3)	104.9, 191.1, −369.2	2.034, 2.045, 2.129
$N_aN_\epsilon;N_aN_\epsilon$ (C_i)[#]	CuHis (7.3)	−12.6, 87.1, −519.3	2.030, 2.046, 2.126
$N_aN_\epsilon;N_aN_\epsilon$ (C_s)*[#]	CuHis (7.3)	158.4, 170.9, −207.9	2.033, 2.036, 2.115
$N_aN_\epsilon;N_aN_\epsilon$ −2W*	CuHis (7.3)	−45.1, 394.4, 533.9	2.033, 2.064, 2.154
$N_aN_\epsilon;N_aN_\epsilon$-fix	CuHis (7.3)	33.4, 48.5, −454.3	2.049, 2.051, 2.167
$N_aN_\epsilon;N_aO_c$		13.9, −33.3, −570.0	2.034, 2.044, 2.131
$N_aN_\epsilon;N_\epsilon O_c$	CuHis B−Y	−33.5, 34.0, −553.0	2.035, 2.049, 2.151
$N_aN_\epsilon;N_\epsilon O_c$+*	CuHis B−Y	−101.1, 233.8, 287.8	2.039, 2.051, 2.143
$N_\epsilon N_a;O_c;O_w$[#]	CuHis (3.8), CuHis A−Y	3.7, −20.1, −569.8	2.043, 2.047, 2.156
$N_\epsilon N_a;O_c;O_w$+[#]	CuHis (3.8), CuHis A−Y	−30.4, −34.8, −532.8	2.043, 2.046, 2.154
$N_\epsilon;O_w;N_\epsilon O_c$		12.8, 128.9, −438.5	2.038, 2.066, 2.188
$N_a;O_w;N_\epsilon O_c$*		−126.3, 350.1, 459.0	2.039, 2.060, 2.175
$N_aN_\epsilon;N_aN_\epsilon;O_w$	CuHis (7.3)	73.0, 155.7, −412.7	2.040, 2.056, 2.151
$N_aN_\epsilon;O_w;N_aN_\epsilon;O_w$	CuHis (7.3)	120.3, 212.3, −387.4	2.040, 2.057, 2.153

[a] The structures marked with * gave unreasonable calculated Cu hyperfine values. These are marked with open triangles in Figure 7b. Those marked with [#] gave bad g_{zz}-values and were also marked with open triangles in Figure 7a.

studied in detail in an earlier publication.[6] These, together with the present HYSCORE data and the results of the solution models, confirm the structure suggested earlier for complex B (see Figure 1c). In contrast, complex A is not a mono-complex as suggested earlier but a bis-complex with a structure similar to that of the CuHis(3.8), shown in Figure 1d with the zeolite oxygen replacing the water ligand. The similar ^{13}C coupling of complexes A and B indicate that the ^{13}C hyperfine coupling is not sensitive to whether the binding mode of the histidine ligands is $N_\epsilon O_c$ or O_c. Table 2 summarizes the experimentally determined hyperfine tensors of the various nuclei in the CuHis complexes investigated.

DFT Calculations. A. Copper Hyperfine and g-Tensor Calculations. A critical factor in the prediction of the hyperfine couplings is the quality of the optimized structures, namely, how well do they represent the real structure. When an X-ray structure is available, it can be used as a reliable starting geometry. Otherwise, as in our case, molecular mechanics methods or simply "chemical intuition" should be invoked in order to set the starting geometry. Since only local, rather than global, minima are calculated, the initial coordinates (as well as the symmetry and other parameters such as basis sets and functional) might have a considerable effect on the final structure. Here we have used the agreement between the calculated and experimental copper hyperfine and g-tensor parameters as an indication for the quality of the optimized structure, under consideration of the known system deficiencies of the employed methods. For this purpose we used as a reference two recent studies,[21,30] in which the performance of the coupled perturbed Kohn−Sham (CP−KS) formalism on various paramagnetic compounds with known structures was tested. The results for the copper compounds were selected and plotted together with our calculations in Figure 7a,b. These calculations were done including spin−orbit coupling terms,[21,30] and the results are given in Table 3. We chose to plot Δg_{zz} (the deviation from g_e, in parts per thousand (ppt)) and A_{zz}(Cu), which are most sensitive to the structure and their experimental values can be determined with high accuracy. Figure 7a shows that the values calculated with B3LYP for the reference compounds are well underestimated, but the deviation seems to be system-

atic. The deviations of the values calculated for some of our structures from the ideal line are comparable to those of the reference compounds, and therefore these were considered as accepted. In contrast, some of our calculated values are outside the accepted error limit.[78] These are marked in Table 3 as # and as open triangles in Figure 7a. Similarly, for A_{zz}(Cu), there are several structures with values which are well outside the acceptable error range or have the wrong sign. These are noted by * in Table 3 and marked by triangles in Figure 7b (here we allow a larger deviation, ∼30%, than that of the spread of the reference points). These structures, therefore, are not good models for the CuHis complexes discussed in this work. After this preliminary selection of possible structures, several candidates remain, which could represent the experimentally observed CuHis complexes. Since the g-tensor and A(Cu) values cannot be used to distinguish between these possibilities, additional criteria must be invoked. Below, we will further narrow down the possible structures by studying their relative energies and, more importantly, their predicted ligand hyperfine couplings which are better reporters of the specific geometric structure than the g-tensor or the central metal hyperfine tensor.

B. Possible Configurations of the $N_aN_\epsilon;N_aN_\epsilon$ Bis-Histamine Complex. Analyzing the differences in the hyperfine couplings of the various structures, we chose to concentrate on H_α and [13]C_c because they have the lowest experimental uncertainties and their a_{iso} values are relatively large. High quality data are also available for the remote nitrogen N_δ and H_ϵ, and the agreement between the experiment and calculation is good. These couplings are relatively small and straightforward to interpret, since they are unique for equatorial N_ϵ coordination, but they are rather insensitive to the specific coordination mode. Although the N_a coordination is easily identified by the large coupling of H_a, the accurate determination of the complete hyperfine tensor of H_{a1} and H_{a2} is somewhat ambiguous due to the overlap of their powder patterns.[7] Nonetheless, the calculated values are generally in the order of the experimental values.

The $N_aN_\epsilon;N_aN_\epsilon$ mode can, in principle, assume either a trans (C_2 or C_i point group symmetries) or cis configuration (C_s), therefore all three conformations were initially considered, and their relative stabilities in a water solution were compared. The

(77) Although there is a 30% contribution of complex A in this sample, the relative intensity of the ^{13}C peaks compared to that of the [27]Al signal indicates that the majority of the ^{13}C peak intensity originates from complex B and the contribution of complex A is minor.

(78) The rejection was done by finding a best fit linear relationship for the reference samples and labeling as bad points the ones that deviate from this line by more than 30%, which approximately represent the span of the references compounds.
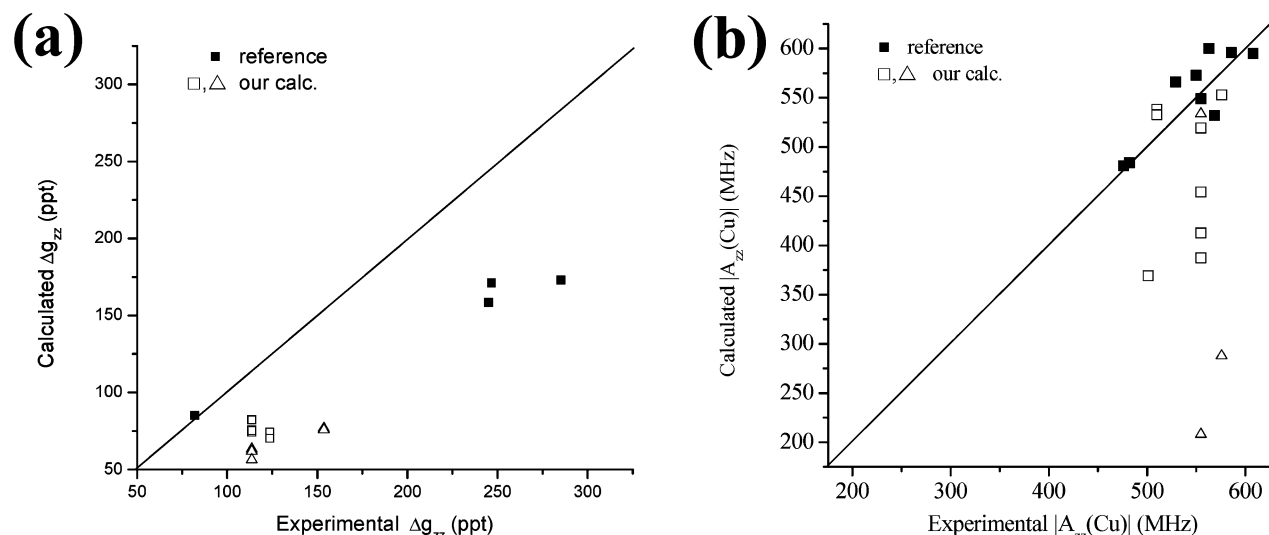
Figure 7. Comparisons of the calculated Δg_{zz}(a) and A_{zz}(Cu) (b) values of various Cu(II)-containing molecules and complexes. The reference data for Δg_{zz} were taken from ref 21 and for A_{zz}(Cu) from ref 30. The solid line represents the ideal fit, $x = y$. All our calculations are listed in Table 3. The open triangles represent structures with values that are not within the accepted error range. The open triangle in part b which is near the solid line was rejected due to its wrong sign.

Table 4. Calculated Hyperfine Coupling Tensors for Alternative Complexes with a Bis-Histamine Coordination (C_2 Symmetry)

type of ligands	$N_aN_\epsilon;N_aN_\epsilon$	$N_aN_\epsilon;N_aN_\epsilon$-fix
energies[a]	0	−6.2
hyperfine, MHz	$a_{iso}, T_{xx}, T_{yy}, T_{zz}$	$a_{iso}, T_{xx}, T_{yy}, T_{zz}$
H_{a1}	−6.07, −8.05, −2.34, 10.4	−4.35, −7.95, −1.23, 9.18
H_{a2}	2.62, −7.41, −2.07, 9.49	1.58, −8.73, −0.74, 9.46
H_α	5.99, −2.55, −1.80, 4.35	6.71, −1.48, −1.43, 2.91
H_ϵ	1.11, −2.41, −1.41, 3.82	1.32, −2.36, −1.31, 3.67
N_a	26.7, −5.08, −5.02, 10.1	24.11, −4.99, −4.82, 9.81
N_ϵ	49.7, −4.22, −3.21, 7.43	36.34, −3.80, −3.13, 6.92
N_δ	2.35, −0.34, −0.07, 0.40	2.14, −0.33, −0.12, 0.44
C_c	3.76, −1.52, −0.76, 2.29	0.15, −0.42, −0.27, 0.69

[a] COSMO relative energies in kcal/mol.

C_s symmetry has already been excluded based on its calculated A_{zz}(Cu) values (see above). Moreover, its relative stability in solution, obtained using the COSMO model showed that the cis isomer is less stable than both trans isomers by 6 kcal/mol. This is expected, considering the higher proximity of the two negatively charged carboxyl groups. The solution energies of the C_2 and C_i trans configuration, however, were found to have the same values (within 0.001 kcal/mol). A comparison of the ligand hyperfine values with the available experimental parameters, in particular, $a_{iso}(H_\alpha)$ and $a_{iso}(C_c)$, also favored the two trans configurations. Selecting between the two latter conformers (C_2 and C_i) is not straightforward, as both showed a similar degree of agreement with the experiments. Moreover, the differences between the two symmetries are rather small with respect to the changes induced by variation of the coordination mode. Therefore, both structures are as likely to represent the CuHis(7.3) solution model. For the rest of the manuscript, we selected (arbitrarily) the C_2 isomer, which will be denoted as $N_aN_\epsilon;N_aN_\epsilon$ without any further reference to its symmetry.

The most significant deviation between experiment and theory in the $N_aN_\epsilon;N_aN_\epsilon$ complex is the large $a_{iso}(C_c)$ (see Table 4), which may be attributed to artifacts in the DFT calculations introduced by free charges on the oxygen atoms. These could be significantly diminished by reoptimizing the structure with two additional water molecules that are placed near the charged
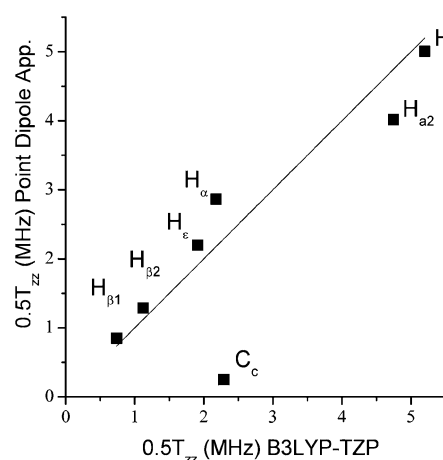
Figure 8. T_{zz} calculated using the point-dipole approximation and the distances determined from the optimized structure in comparison with T_{zz} obtained by DFT for the $N_aN_\epsilon;N_aN_\epsilon$ complex. The linear curve corresponds to $y = x$.

carboxylate groups, referring to it as $N_aN_\epsilon;N_aN_\epsilon$ −2W. The spin densities on the carboxyl oxygen with the large spin density indeed become smaller (decreased from 2.7% to 0.47%), and the calculated $a_{iso}(C_c)$ and $T_{zz}(C_c)$ values of the new structure are in better agreement with the experimental data, but a decrease in $a_{iso}(H_\alpha)$ deteriorates the overall agreement. More importantly, the Cu hyperfine values are far from the experimental values and therefore it has been rejected (see Table 3 and Figure 7). A more satisfactory model of these effects would require the use of a large solvent cage in combination with molecular dynamics techniques which is outside the scope of this paper.

The deviations of the predicted T_{zz} values for all ligand nuclei of the $N_aN_\epsilon;N_aN_\epsilon$ structure from those computed using the point-dipole approximation (eq 3), where r is taken from the optimized structures, are presented in Figure 8. The correspondence is good for distant nuclei, such as H_β, and generally deteriorates as the distance becomes smaller. For C_c there is a large deviation from the ideal curve, and we attribute it to the overestimated spin density on the carboxyl (see above). Finally, the deviation from
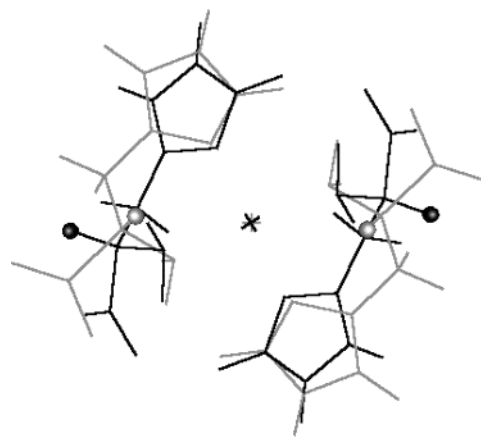
axiality for H_α is relatively small, as compared to that of H_{a1} and H_{a2}, which is in agreement with the experimental results. Therefore, the deviations from the calculated T_{zz} values from the experimental ones indicate that the optimized structure does not represent well the real structure. To improve the agreement with the experimental hyperfine couplings of the $N_aN_\epsilon;N_aN_\epsilon$ structure, we have modified the structure by the addition of axial water ligands, tested the effect of protonation of the carboxylate and finally optimized the structure under geometrical constraints obtained from the experimental results. These are presented next.

C. Effect of Axial Ligation. So far the structures studied by DFT were limited to four equatorial ligands, yet Cu(II) is known to form also five- and six-coordinated complexes.[79] Therefore, we have also explored the effect of axial ligation on the stability and ligand hyperfine coupling by adding one or two water ligands at axial positions to produce $N_aN_\epsilon;N_aN_\epsilon;O_w$ and $N_aN_\epsilon;O_w;N_aN_\epsilon;O_w$. The possibility of axial coordination of the two histidine carboxyl groups to form a six-coordinated complex of the form $N_aN_\epsilon O_c;N_aN_\epsilon O_c$ was tested as well. Such a coordination mode was suggested by Szabó−Plánka and co-workers.[1]

The addition of axial water ligands to the $N_aN_\epsilon;N_aN_\epsilon$ results in complexes which are thermodynamically more stable in solution; each water coordination in solution releases about 10 kcal/mol. This is obviously an effect of doing the calculations in a vacuum. In the real solvent, the solvation energy of the water molecules should be taken into account to estimate realistic energetics for such a reaction. This is, however, not necessary in the present context, since we are focusing on spectroscopic parameters. The water axial ligation affected mostly the hyperfine couplings of $H_{a1,2}$, the magnitude of which has significantly decreased (see Table S1). This seems to correlate with the deviation in the N_x-Cu-N_x ($x = a$ or ϵ) angle from $180°$, namely the Cu(II) and the four equatorial ligands do not lie in one plane any longer. For example, N_a-Cu-N_a and $N_\epsilon-Cu-N_\epsilon$ are $171°$ and $175°$, respectively, for $N_aN_\epsilon;N_aN_\epsilon$ and are reduced to $166°$ and $159°$ for $N_aN_\epsilon;O_w;N_aN_\epsilon;O_w$. Interestingly, the effect of one water ligand is greater than that of two, which is attributed to the reduced symmetry of the $N_aN_\epsilon;N_aN_\epsilon;O_w$ complex (C_1) as compared to the other two complexes (C_2). The effect on other hyperfine values is smaller. Comparison of the a_{iso} values with the experimental ones shows that calculated $a_{iso}(H_a)$ values are too small. Whether this implies that the CuHis(7.3) complex does not have axial water ligand(s) is still an open issue.

Attempts to optimize the $N_aN_\epsilon O_c;N_aN_\epsilon O_c$ complex under C_i symmetry constraints resulted in a very weak coordination of the two carboxyl ligands; the final $Cu-O_c$ distance was 4.12 Å while in the starting geometry the distance was set to 2.80 Å. The structure and the hyperfine parameters were practically the same as those calculated for the $N_aN_\epsilon;N_aN_\epsilon(C_i)$ structure; hence we conclude that the histidine ligand is more stable as a bidentate rather than a tridentate ligand.

D. Protonation Effects. The three binding sites in the histidine ligand are basic and can be protonated;[80] hence, the effective charge of the complex is strongly pH dependent. In

(79) Hathaway, B. J.; Billing, D. E. *Coord. Chem. Rev.* **1970**, *5*, 143−207.
(80) In fact the two imidazole nitrogens undergo rapid tautomeric exchange. The pyridine rather than the pyrrole nitrogen is, however, more likely to coordinate to copper. (See Sundberg, R. J.; Martin, R. B. *Chem. Rev.* **1974**, *74* (4), 471.)

Figure 9. Comparison between the optimized $N_aN_\epsilon;N_aN_\epsilon$ (gray) and $N_aN_\epsilon;N_aN_\epsilon$-fix (black) structures. The copper sites (+) overlap, and the spheres represent the H_α protons.
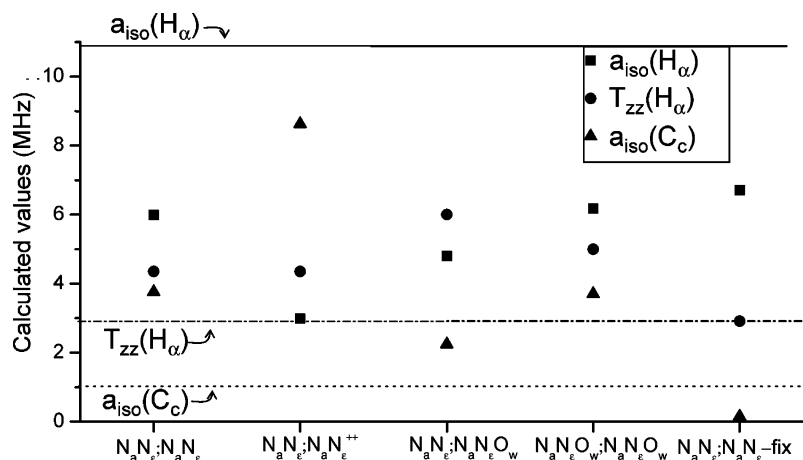
solution, the available pK_a values can be used to determine the protonation state of each group ($pK_a(O_c) = 3.1$, $pK_a(N_\epsilon) = 6.5$, $pK_a(N_a) = 8.0$). But since pK_a values depend on the ionic strength and the microenvironment of the ionizable group, the final state of each basic group, particularly when encapsulated in zeolites, cannot be predicted. Therefore, the effect of protonation on several types of complexes, independent of the prediction based solely on the experimental solution pH, was tested.

The $N_aN_\epsilon;N_aN_\epsilon$ structure was reoptimized with two protons on the carboxylic groups, thereby creating a doubly charged complex $(N_aN_\epsilon;N_aN_\epsilon)^{++}$. The latter was selected, despite the low pK_a value of the carboxylic groups to avoid dangling anions (COO⁻ groups), which tend to produce artifacts in DFT calculations. While protonation causes only subtle structural changes, for example, the maximum bond length variation is 0.12 Å, the changes in the spin distribution are significant (see Figure S3). The major change occurs at the carboxylate oxygen, where the proton causes a considerable decrease in the spin density on the adjacent oxygen atom. The changes are manifested in the a_{iso} values of most nuclei (see Table S1); for example, in the case of H_α, it decreases by as much as 50%, deteriorating the agreement with the experimental results.
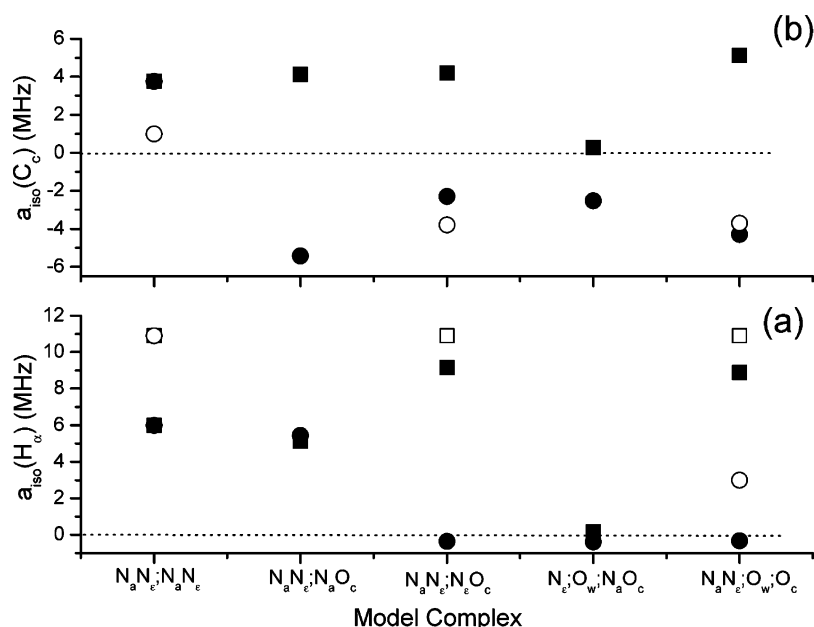
E. Optimization under Experimental Constraints. In a final attempt to improve the agreement with the experimental hyperfine couplings, the $N_aN_\epsilon;N_aN_\epsilon$ structure was reoptimized by fixing the $Cu-H_\alpha$ distance at $r_{(Cu-H\alpha)} = 3.87$ Å, which was derived from the experimental $T_{zz}(H_\alpha) = 2.6$ MHz using the point-dipole approximation (eq 3), while all other structural parameters were kept free. The hyperfine couplings are listed in Table 4. Surprisingly, despite the 0.85 Å increase in the $Cu-H_\alpha$ distance relative to $N_aN_\epsilon;N_aN_\epsilon$, the new $a_{iso}(H_\alpha)$ value increased from 6 to 6.7 MHz, thereby improving the agreement with the experiment. Similarly, $a_{iso}(C_c)$ is much closer to the experimental value. In terms of relative solution energies, the new structure is also more stable (in solution) than the $N_aN_\epsilon;N_aN_\epsilon$ (C_2) structure by 5 kcal/mol. Figure 9 shows an overlay of the original $N_aN_\epsilon;N_aN_\epsilon$ (C_2) and the newly optimized structure ($N_aN_\epsilon;N_aN_\epsilon$-fix). The difference between the structures is mainly in the angle between the $C_\alpha-H_\alpha$ bond and the $C_\alpha-Cu$ vector, implying that the orientation of the $C_\alpha-H_\alpha$ bond has a strong effect on $a_{iso}(H_\alpha)$, as expected from the hyperconjugation mechanism.[81] Figure 8 shows that, for a structure for

Figure 10. Comparison of the calculated $a_{iso}(H_\alpha)$, $T_{zz}(H_\alpha)$, and $a_{iso}(C_c)$ for various $N_aN_\epsilon;N_aN_\epsilon$ coordination modes. The solid, dashed, and dotted lines represent the corresponding experimental values of CuHis(7.3), respectively.

Figure 11. Comparison of the calculated $a_{iso}(H_\alpha)$ (a) and $a_{iso}(C_c)$ (b) of the various CuHis complexes along with some experimental values. Filled squares and circles correspond to calculated values for ligands 1 and 2, respectively, while empty symbols correspond to experimental values.

which DFT produces $T_{zz}(H_\alpha) = 4.35$ MHz, the point-dipole approximation introduces a deviation of -1.3 MHz, amounting to a significant distance error of $+0.3$ Å. In contrast, for T_{zz} similar to the experimental $T_{zz}(H_\alpha)$ value, Figure 8 shows a smaller deviation of about -0.3 MHz, which amounts to only a 0.1 Å error in the distance, thus justifying this approach. This is verified by the calculated **T** which is indeed very close to having axial symmetry with $T_{zz}(H_\alpha) = 2.91$ MHz. In principle, if a better structure is still desired, several optimizations can be carried out with $r_{(Cu-H\alpha)}$ in the range of 3.87 ± 0.1 Å.

To summarize this part, Figure 10 compares the calculated hyperfine couplings of H_α and C_c of the various Cu(His)$_2$ complexes involving the $N_aN_\epsilon;N_aN_\epsilon$ coordination mode with the experimental values of CuHis(7.3). While the hyperfine couplings of these nuclei are very sensitive to subtle changes in the geometry, those of H_ϵ and N_δ are insensitive and in very good agreement with the experimental results. The structure which yields the best agreement with the experiment, in terms

(81) Wertz, J. E.; Bolton, J. R. *Electron Spin Resonance: Elementary Theory and Practical Applications*; McGraw-Hill: USA, 1972; pp 168–170.

of ligand hyperfine coupling, is $N_aN_\epsilon;N_aN_\epsilon$-fix. While its g_{zz} value also shows better agreement compared to all $N_aN_\epsilon;N_aN_\epsilon$ structures, the $A_{zz}(Cu)$ value is better than some but not as close to the experimental value as that of $N_aN_\epsilon;N_aN_\epsilon$ (C_i) (see Table 3).

F. Hyperfine Couplings of Other Cu(His)$_2$ Complexes. The calculated hyperfine components of all ligand nuclei of Cu-(His)$_2$ complexes with equatorial carboxylate coordination $N_aN_\epsilon;N_aO_c$, $N_aN_\epsilon;N_\epsilon O_c$, where both histidine ligands are bidentate, and of complexes of the form Cu(His)$_2$·H$_2$O: $N_\epsilon;O_w;N_\epsilon O_c$, $N_aN_\epsilon;O_c;O_w$, where one ligand is monodentate, are given in Tables S2 and S3. The $N_a;O_w;N_\epsilon O_c$ structure produced unacceptable Cu hyperfine values and therefore will not be considered. Figure 11 shows the dependence of $a_{iso}(H_\alpha)$ and ($^{13}C_c$) on the coordination mode and compares them to the experimental value, when available. A comparison of the calculated hyperfine values of these various complexes along with $N_aN_\epsilon;N_aN_\epsilon$-fix reveals the following:

(1) $a_{iso}(H_{a1,2})$ is large only when N_a is coordinated. For the N_aN_ϵ coordination, there is a large difference between $a_{iso}(H_{a1})$

and $a_{iso}(H_{a2})$, while the anisotropic part is similar. In contrast, for N_aO_c and $N_a;O_w$, the two a_{iso} values are closer. The range spanned by $a_{iso}(H_{a1})$ is relatively small, -6.2 ± 1.8 MHz (30%), whereas that of $a_{iso}(H_{a2})$ is very large, -4.35 to 2.39 MHz. The anisotropic components are fairly constant and vary within less than 10% and are considerably larger than the experimental values. This suggests that the orientation of H_{a2} is such that small changes strongly affect its a_{iso} value. The sign of $a_{iso}(H_{a1})$ is in good agreement with the experiment but that of the anisotropic part is not. This however could be due to the uncertainty of the simulations of the H_a protons as mentioned earlier.

(2) $a_{iso}(H_{\alpha})$ is large and positive as long as N_a is coordinated to the Cu(II) and it is sensitive to the coordination mode of the second histidine (see Figure 11). Its range is 7 ± 2 MHz (28%), and although the large positive values agree with the experiment, there are some significant differences: the calculated $a_{iso}(H_{\alpha})$ is underestimated for the $N_aN_\epsilon;N_aN_\epsilon$ complexes and it is closer to the experimental value for $N_aN_\epsilon;N_\epsilon O_c$ and $N_aN_\epsilon;O_c;O_w$. In fact, the experimental value is not sensitive to the coordination mode of the second histidine molecule. Moreover, the experimental results point to a large a_{iso} and small T_{zz} for a histamine N_aN_ϵ coordination,[7] rather than a single N_a coordination as suggested by the calculation. The anisotropic part shows a larger range of variation, which reflects the flexibility of the C_{α} region. In all optimized structures with a N_a coordination, except for $N_aN_\epsilon;N_aN_\epsilon$-fix and $N_aN_\epsilon;N_aO_c$ (second ligand), the anisotropic part is significantly larger than in the experiment, indicating that the Cu(II)$-H_{\alpha}$ distance is too short in these optimized structures. This is attributed again to some conformational freedom at the C_{α}, which leads to a number of possible conformations and thereby to different hyperfine couplings.

(3) $a_{iso}(C_c)$ for an equatorially coordinated carboxylate is negative and varies in the range of -3.9 ± 1.6 MHz (41%), depending on the coordination mode (Figure 11). This is consistent with the experimental results in terms of both magnitude and sign (Table 2). Furthermore, the size of the anisotropic components and the large deviation from axial symmetry are also in good agreement with the experiment. The large positive $a_{iso}(C_c)$ for the free O_c (4–5 MHz) in some structures is, however, unexpected. Indeed, this prediction agrees only in term of the sign but not with the magnitude of the experimental value of $^{13}C-CuHis(7.3)$ ($N_aN_\epsilon;N_aN_\epsilon$), which is significantly smaller (1 MHz). We attribute some of this inconsistency to the sensitivity of the spin density on the free COO^- to the charge, which suggests a calculation artifact. Interestingly, the $N_aN_\epsilon;N_aN_\epsilon$-fix structure, which includes the negative charges on the oxygen atoms, yields an $a_{iso}(C_c)$ value which is in a reasonable agreement with the experiment.

(4) When N_ϵ is coordinated, $a_{iso}(H_\epsilon)$ ranges between 1.3 ± 0.45 MHz (47%). This range is small, considering the small hyperfine values. The range of the anisotropic components is even smaller and all values are close to the experimental ones. The behavior of N_δ is very similar to that of H_ϵ, and the calculated values are close to the experimental values.[6,51,82] $a_{iso}(N_\epsilon)$ is usually larger than $a_{iso}(N_a)$, and its variation range is relatively small, 41 ± 5 MHz (12%), similar to the other nuclei of the imidazole group. This shows that the hyperfine interactions of H_ϵ, N_ϵ, and N_δ are not sensitive to the other coordinated

Table 5. Summary of All the Experimental β Angles and the Calculated Values for Selected Optimized Models

ligand	experimental	DFT	DFT, range
H_α in CuHis(7.3)	60°	50° [a]	25–89° [b]
H_ϵ in CuHis(7.3)	70°	79° [a]	64–92° [b]
C_c in CuHis(7.3)	0°	68°	48–80° [b]
C_c in CuHis(3.8)	90°	77° [c]	75–79°

[a] Obtained from the $N_aN_\epsilon;N_aN_\epsilon$-fix structure. [b] The range of all $N_aN_\epsilon;N_aN_\epsilon$ structures calculated in this work (see Tables 4 and S1). [c] The number is the average of the $N_aN_\epsilon;O_c;O_w$ complex and a similar structure including a protonated free amine group, $N_aN_\epsilon;O_c;O_w^+$.

atoms and that the freedom in the position of these nuclei is rather limited once N_ϵ is coordinated.

(5) $a_{iso}(N_a)$ ranges around 32.5 ± 8.5 MHz (26%). Although we have not measured the hyperfine couplings of the coordinated nitrogen atoms, comparison with literature values of similar compounds shows that these are within the expected range.[83]

This comparison shows that the hyperfine couplings of some nuclei are more sensitive to structural variations and that the isotropic hyperfine coupling is more sensitive than the anisotropic part.

G. Orientation of the Hyperfine Tensors. So far we have considered only the magnitude of the hyperfine components, but the orientation of the tensor should be considered as well. Table 5 compares the available experimental β angles with those predicted by DFT. We have compared only the β angle (the angle between the direction of T_{zz} of the relevant ligand nucleus and g_{zz}) because its experimental determination is the most reliable one. The agreement is reasonable, considering an uncertainty of $\pm10°$ in the experimental value. The large deviation for C_c in CuHis(7.3) is attributed to a much larger experimental uncertainty arising from the very small anisotropy.

Correlation between a_{iso} and bond orientations are often very useful. For example, the correlation $a_{iso} \propto \cos^2 \phi$, where ϕ is the OVOH dihedral angle, was recently found for the protons of equatorial water ligands of VO(II).[38] Other examples are the a_{iso} of the cysteine β-protons of type I (blue) and Cu_A copper centers in proteins.[83,84] Accordingly, we looked for a similar correlation between $a_{iso}(H_\alpha)$ and the dihedral (torsion) angle between the planes containing $H_\alpha C_\alpha N_a$ and $C_\alpha N_a Cu$ in the various complexes with histamine coordination (N_aN_ϵ). No correlation was found, indicating that there are additional factors, which vary among the structures and should be considered. Hence, such a correlation should be explored first on a single structure which is subjected to a controlled systematic rotation of the bond.[85] This is beyond the scope of this work.

Conclusions

The carboxyl ^{13}C isotropic hyperfine coupling of an equatorially coordinated carboxylate in Cu(II) glycine and histidine complexes is characterized by a negative hyperfine coupling with a magnitude of 3–4 MHz, as opposed to a small (~1 MHz) and positive value for a free carboxylate in copper histidine. This can be used as a signature for carboxylate coordination to Cu(II) as was shown for the Cu(II) histidine complex in solution at pH = 3.8 and for zeolite Y encapsulated Cu(II) histidine

(82) Kofman, V.; Farver, O.; Pecht, I.; Goldfarb, D. *J. Am. Chem. Soc.* **1996**, *118*, 1201–1206.

(83) Werst M. M.; Davoust, C. E.; Hoffman, B. M. *J. Am. Chem. Soc.* **1991**, *113*, 1533–1538.
(84) Neese, F.; Kappl R., Hütterman, J.; Zumft, W. G.; Kroneck, P. M. H. *J. Bioinorg. Chem.* **1998**, *3*, 53–67.
(85) Arieli, D.; Strohmaier, K. G.; Vaughan, D. E. W.; Goldfarb, D. *J. Phys. Chem. B* **2002**, *106*, 7509–7519.

complexes. In the former, the coordination mode was found to be $N_aN_\epsilon;O_c;O_w$ and, in the latter, depending on the degree of Cu(II) loading, $N_aN_\epsilon;N_\epsilon O_c$ or $N_aN_\epsilon;O_c;O_z$. The determination of ^1H hyperfine couplings of the different ligand protons in the complex are not sufficient to determine the structure unambiguously, since the carboxylate binding remains inconclusive.

The combination of various ENDOR techniques, particularly at a high magnetic field where the sign of the hyperfine coupling can be determined experimentally, with DFT generates a useful toolbox for interpreting the spectroscopic parameters in terms of structure. In this particular example, the DFT calculations provided the motivation for the experimental sign determination of the ^{13}C hyperfine coupling. However, while the agreement between the DFT sign prediction and the experimental sign was excellent for the ^1H and ^{13}C nuclei, the magnitude of the couplings often exhibited significant deviations (in the range of 20−50%). Moreover, the dependence of the calculated values on the coordination mode did not always agree with the experimental trends.

Several factors were found to be responsible for these disagreements: (i) The quality of the optimized structure, which seems to play a major role. This particularly depends on the starting geometry, the symmetry, and potential constraints imposed on the structure. Thus, whenever possible, geometrical constraints based on experimental results should be incorporated into the optimization procedure. (ii) Global and local charge effects; free carboxylate or charged amine groups tend to bias the spin density distribution. Finally, (iii) the relatively strong dependence of the hyperfine coupling constants on the functional used. Other parameters such as solvent inclusion in the optimization and axial ligation were found to be only of minor importance. However, since solvent effects were considered only in the optimization procedure and not on the hyperfine coupling calculation, this issue remains open. Finally, the detailed

experimental information on the hyperfine coupling and *g*-values of various ligand nuclei in different Cu(II) histidine complexes can serve in the future as critical constraints for a better adaptation of exchange-correlation functionals used in DFT for ligand hyperfine calculations. Alternatively, there is also hope that correlated ab initio methods will become efficient enough to study molecules of the size considered here and that such methods represent real improvements of the currently available DFT procedures.

Note Added after ASAP Posting. After this paper was posted ASAP on August 26, 2004, an error in eq 2 was corrected. The corrected version was posted August 31, 2004.

Supporting Information Available: (1) A summary of the general expressions used for the calculations of the hyperfine and *g*-tensors. (2) The dependence of the hyperfine couplings of H_α and H_{a1} of the $N_aN_\epsilon;N_aN_\epsilon$ complex on a series of basis sets and functionals. (3) The effect of the inclusion of a solvent during the structure optimization of this complex on the hyperfine couplings of various ligand nuclei. (4) Tables with the calculated hyperfine couplings of $N_aN_\epsilon;N_aN_\epsilon^{++}(C_2)$, $N_aN_\epsilon;N_aN_\epsilon;O_w$, $N_aN_\epsilon;O_w;N_aN_\epsilon;O_w$, $N_aN_\epsilon;N_aO_c$, $N_aN_\epsilon;N_\epsilon O_c$, $N_\epsilon;O_w;N_\epsilon O_c$, $N_aN_\epsilon;O_c;O_w$. (5) A figure with the spin density distribution in a few structures. This material is available free of charge via the Internet at http://pubs.acs.org.

JA047761C